ISSN 1062-8738, Bulletin of the Russian Academy of Sciences: Physics, 2019, Vol. 83, No. 10, pp. 1275–1281. © Allerton Press, Inc., 2019.
Russian Text © The Author(s), 2019, published in Izvestiya Rossiiskoi Akademii Nauk, Seriya Fizicheskaya, 2019, Vol. 83, No. 10, pp. 1394–1401.

Phase Composition and Magnetic Properties of Fe_2O_3–FeO–Gd_2O_3 Powders after High-Energy Ball Milling and Thermal Treatment

S. V. Salikhov[a], *, S. K. Toleukhanova[a], I. G. Bordyuzhin[a], and A. G. Savchenko[a]

[a] *National University of Science and Technology (MISiS), Moscow, 119049 Russia*

**e-mail: salta_150@inbox.ru*

Received January 10, 2019; revised May 13, 2019; accepted June 27, 2019

Abstract—Comprehensive studies of powders with a nominal composition of 90% [43% Fe_2O_3–57% FeO]–10% Gd_2O_3 are performed via scanning electron microscopy, microscopic X-ray spectral and phase analysis, differential scanning calorimetry, and measuring hysteresis properties. It is shown that the main phases in the powders after high-energy ball milling are magnetite (Fe_3O_4) and an amorphous phase; in addition, the powders contain about 2 vol % wustite (FeO) and less than 1 vol % orthoferrite ($GdFeO_3$). Trends of changes in the phase composition, structure, and hysteresis properties of the annealed powders are identified.

DOI: 10.3103/S1062873819100186

INTRODUCTION

There is growing interest in magnetic materials with nanometer-range sizes due to their unique properties when a macroscopic or bulk microscopic material transforms into a nanosized or nanostructured state. Oxides of the Fe–O system in the nanosized state have a number of features that find application in different fields of science and technology, including medicine. For example, nanoparticles of iron oxide, obtained by different chemical means, are used in targeted drug delivery [1], magnetic hyperthermia [2], as negative T_2 contrast agents (making images darker) in magnetic resonance imaging (MRI) [3, 4], and in magnetic memory devices [5]. Compounds based on gadolinium, including gadolinium oxide (Gd_2O_3) are also being investigated as possible positive T_1 contrast agents (making images brighter) in MRI [6, 7]. For all their usefulness, however, T_1 and T_2 contrast agents have some disadvantages [8]. For instance, T_1 contrast agents based on gadolinium allow us to achieve good contrast enhancement [9], but there is the risk of inducing nephrogenic systemic fibrosis in patients with kidney dysfunction, especially ones who are older [10, 11]. In addition, Gd chelates now being used are removed very quickly from the blood flow. Magnetic nanoparticles of iron oxide have low toxicity; however, the lack of tissue specificity, cases of low background intensity, and ambiguity in distinguishing various endogenous objects (e.g., deposits of calcium or iron, lipids, blood clots, air bubbles, or bleeding) that are often observed limit their use [12].

The problem of creating contrast agents free of these drawbacks is of great importance today. Dual-modal T_2–T_1 contrast agents, which simultaneously have high values of longitudinal (r_1) and transverse (r_2) relaxivities and low r_2/r_1 ratios are especially promising. Their use would greatly improve the efficiency and accuracy of MRI. Information has recently appeared in the literature where the development and synthesis of hybrid T_2–T_1 contrast agents using different chemical means are described; examples include obtaining core–shell nanoparticles with cores made of magnetic iron oxides or ferrites, and shells based on different rare-earth metal compounds, including gadolinium [13, 14] or water-soluble and biocompatible monodisperse ultrasmall ($D = 3.3 \pm 0.5$ nm) magnetic nanoparticles of iron oxide [8]. To some degree, these systems meet the mentioned requirements.

In our opinion, however, magnetic iron oxides alloyed with rare-earth metals (REMs) are more promising as dual-modal T_2–T_1 contrast agents. Until now, the formation of stable phases with spinel structure had not been achieved reliably, despite numerous attempts to synthesize REM-doped magnetic iron oxides chemically [15, 16]. To determine the possibility of such systems existing, in this work we study the effect annealing has on the phase composition, structure, and magnetic properties of nanostructured powders of gadolinium and iron oxide after their joint high-energy milling.

Table 1. Results from our chemical analysis of the powders in the initial state and after high-energy mechanochemical synthesis (HMCS)

Element	Chemical composition of the powders, wt %	
	before HMCS	after 15 h of HMCS
Fe	67.0	68.6
Gd	8.7	8.8
O	24.3	22.6

EXPERIMENTAL

Materials

Nanostructured powders based on iron oxides alloyed with gadolinium were synthesized from hematite Fe_2O_3 (standard STP TU KOMP 1-526-12), wustite FeO (TU 6-09-1404-76), and gadolinium oxide Gd_2O_3 (TU 48-4-524-89). Powder mixtures with a nominal composition of 90% [43% Fe_2O_3–57% FeO]–10% Gd_2O_3 were used to ensure the reaction $Fe_2O_3 + FeO \rightarrow Fe_3O_4$ during high-energy mechanochemical synthesis and alloying with gadolinium.

Acquisition and Thermal Treatment of the Powders

High-energy milling of the powder mixtures was performed in a water-cooled Aktivator 2S planetary ball mill over 15 h in an atmosphere of purified argon and at shell and disc rotation rates of 800 and 400 rpm, respectively. Milling balls made of stainless steel and having diameters of 6 to 15 mm were used. The mass of the balls was 300 g, and the mass of the powder sample was 15 g. To prevent powder agglomeration, 0.1 mL of oleic acid was added into the mill.

The mechanically activated powders were annealed for 30 min inside a VS-4-10.5 electric oven in an Ar atmosphere (99.998%, TU 6-21-12-94) and the temperature range of 200 to 900°C.

Procedure

The elemental composition of the initial materials and the studied powders was determined via microscopic X-ray spectral analysis on a JSM-IT500 scanning electron microscope (SEM) with an accelerating voltage of 20 kV.

Differential scanning calorimetry (DSC) and thermogravimetric analysis (TGA) of the powders subjected to high-energy mechanochemical synthesis (HMCS) were performed on a NETZSCH STA 449 F3 instrument. The powders were heated and cooled in an argon atmosphere in the temperature range of ambient to 900°C at a rate of 10°C/min.

X-ray structural analysis (XRD) of the initial materials and the studied powders was conducted on a DRON-4 diffractometer (CoK_α radiation, $\lambda = 0.179$ nm, $U = 40$ kV, $I = 30$ mA). The input slit on the perimeter of the goniometer was 1 mm wide, as was the counter's input slit. A graphite monochromator (002) was applied to the diffracted ray. The range of diffraction angles 2θ was 10° to 120° with a step of 0.1°; period of exposure for each point was 4 s. Special cells were used for analysis: the powder was put inside and pressed with the addition of ethanol, allowing us to avoid additional lines from a binding agent and reducing the background level. Qualitative and quantitative phase analyses were performed according to Rietveld using specially developed Phan% software [17]. The sensitivity of phase analysis was 1 vol %, and the statistical error in determining the phase content did not exceed 2%.

Hysteresis properties of the powders were measured on a VSM-250 vibration magnetometer in fields of up to 2 T at room temperature. The error in measuring the specific magnetization was ±0.003 A m^2.

RESULTS AND DISCUSSION

Investigating the Chemical Composition and Morphology of the Powders

Results from our microscopic X-ray spectral analysis are presented in Table 1. They show the content of gadolinium in powders remained virtually the same after 15 h of high-energy milling, compared to the initial mix with a nominal composition of 90% [43% Fe_2O_3–57% FeO]–10% Gd_2O_3 (8.7% in the initial composition and 8.8% in the powders after HMCS). The amount of iron grew slightly, but the ratio of the mass fractions of iron and gadolinium rose by just 0.1 wt %, from 7.7 to 7.8%. The oxygen content in the powders fell after HMCS, and the drop (1.7 wt %) corresponds to the abovementioned increase in the iron content (nearly 1.6 wt %). We may assume that all of the observed changes were due to the milling of the balls' material during the lengthy grinding process in the protective atmosphere [18].

Figure 1 shows microscopic images of the powders after 15 h of high-energy milling obtained on a SEM with magnifications of 1000 and 2000. The powder particles are quasispherical, exhibit a wide size dispersion (the sizes of the biggest and the smallest particles differ by nearly three orders of amplitude), and are prone to agglomeration (almost all large particles are surrounded by coatings of smaller particles).

DSC curves from heating and cooling the powders subjected to HMCS for 15 h are presented in Fig. 2. The heating DSC curve in the range of 625 to 695°C displays a broad exothermic peak that can be attributed to the magnetite–wustite transformation. The considerable deviation of the temperature of this transformation (the peak position shifts by almost 100°) from that of the analogous equilibrium transformation of bulk magnetite to wustite (560°C [19]) can

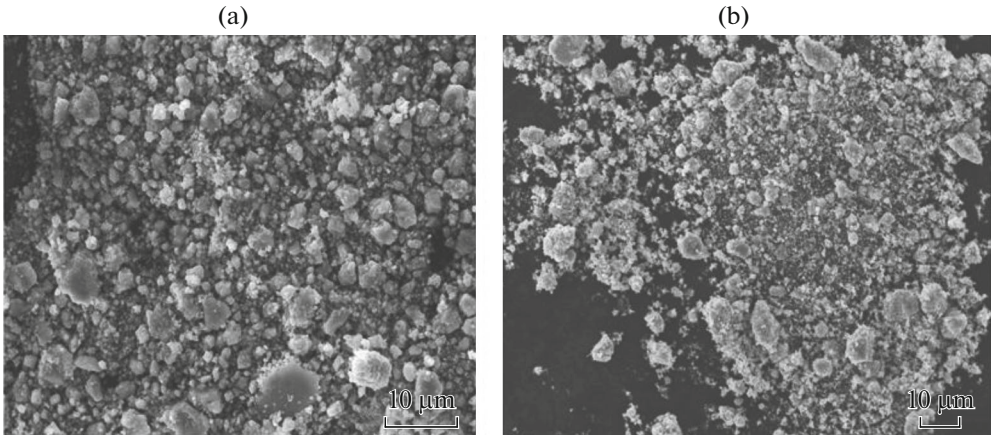

Fig. 1. SEM images of the powders after 15 h of HMCS for the mix with a nominal composition of 90% [43% Fe_2O_3–57% FeO]–10% Gd_2O_3, obtained at magnifications of (a) 1000 and (b) 2000.

be explained by the greater stability of the low-temperature phase in the nanodispersed state. The inverse transformation (showing a much smaller thermal effect) observed upon cooling occurs only 15°–20° lower that the equilibrium temperature; i.e., it is analogous to the transformation in bulk FeO.

Phase Composition and Structure

X-ray diffraction spectra of the powders in the initial state (the oxide mix with a nominal composition of 90% [43% Fe_2O_3–57% FeO]–10% Gd_2O_3) and after annealing the HMCS-powders in the temperature range of 200–900°C are plotted in Fig. 3. The diffraction peaks on the spectra of the HMCS-powders annealed at temperatures below 600°C are notably broadened, testifying to the high degree of dispersion of the coherent scattering regions (CSRs) in the main phase component (corresponding dependences of the CSR sizes on the annealing temperature are shown in Fig. 4). The main phase was magnetite (space group *Fd3m*; the volume fraction of Fe_3O_4 in the HMCS powders was about 97%) (see Fig. 5). Among the initial oxides (Fe_2O_3, FeO, Gd_2O_3), only peaks of wustite are observed in the powder spectrum after 15 h of HMCS, though its relative content is low: around 2 vol % (Fig. 5).

In addition to Fe_3O_4 and FeO, traces of a new phase (no more than 1 vol %) are seen in the diffraction spectrum: orthoferrite $GdFeO_3$ with a distorted perovskite-type structure (space group *Pcmn*). Note that if all gadolinium oxide present in the initial mix were transformed into orthoferrite, the content of the $GdFeO_3$ phase would be at least 14 vol %. The observed small amount of $GdFeO_3$ and the absence of gadolinium oxide diffraction peaks on the spectra of HMCS-powders suggests that (1) Gd was partially dissolved in the spinel lattice, as is confirmed by an increase in the magnetite lattice period after HMCS (Fig. 6), and (2) participated in the formation of another phase that was X-ray amorphous, according to the nonlinear background at angles $2\theta < 50°$.

Figure 5 shows the effective volume content of magnetite $v_{Fe_3O_4}$ (remember, we did not allow for the possible presence of the X-ray amorphous phase in the powders after HMCS, or a drop in its content during annealing) remained virtually the same after annealing of the HMCS powders below 600°C, though the lattice parameter of Fe_3O_4 (Fig. 6) at the abovementioned temperatures gradually returned to the tabular value (a = 0.8397 nm [20]; shown by the dashed line in the figure). At the same time, we observe an increase in the volume fraction of the orthoferrite phase $GdFeO_3$ that reaches 14 vol % after annealing at 900°C (Fig. 5). Along with the changes in the Fe_3O_4 lattice parameter (Fig. 6), this proves that gadolinium was dissolved in the magnetite lattice and in the amor-

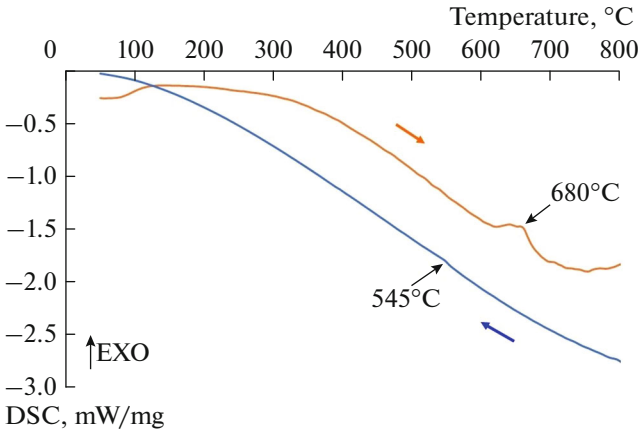

Fig. 2. DSC curves upon heating and cooling the powders after 15 h of HMCS for the mix with a nominal composition of 90% [43% Fe_2O_3–57% FeO]–10% Gd_2O_3.

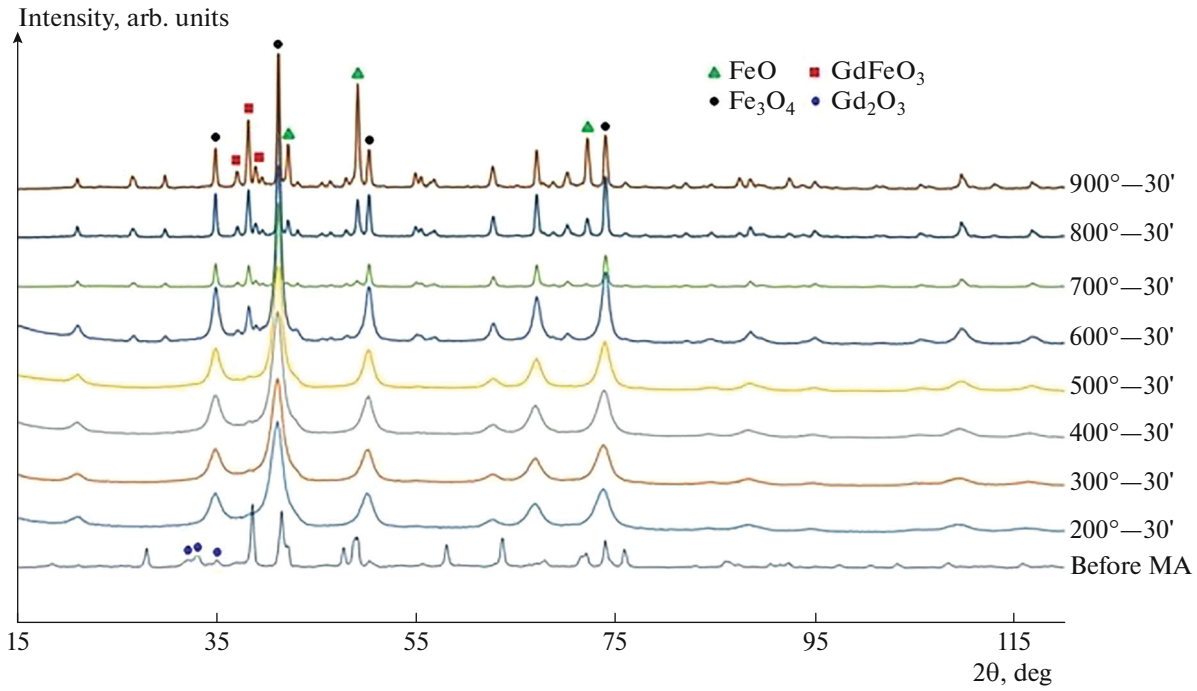

Fig. 3. X-ray diffraction spectra of the powders in the initial state (the oxide mix with a nominal composition of 90% [43% Fe_2O_3–57% FeO]–10% Gd_2O_3) after 15 h of HMCS and 30 min of heating the HMCS powders in the temperature range of 200 to 900°C.

phous phase during HMCS, and was separated during annealing at temperatures above 600°C.

Another feature of the annealing of HMCS powders revealed by X-ray phase analysis (Fig. 5) is that the magnetite–wustite transformation occurs at temperatures higher than 600°C, which agrees with the conclusions drawn by analyzing the DSC/TG data (Fig. 3), while the equilibrium temperature of this transformation is 560°C, according to the Fe–O diagram [19]. In addition to the above, we suggest this discrepancy was due to (1) atmospheric conditions in annealing the HMCS powders (Ar), which could have differed from those used in building the equilibrium state diagram, and (2) a rise in the temperatures at which the magnetite phase was stable, due to the presence of gadolinium ions in the lattice.

Table 2. Hysteresis properties of the HMCS powders in the initial state and after 30 min of annealing in the temperature range of 200–900°C

T_{ann}, °C	H_{ci}, kA/m	σ_r, A m^2/kg	σ_{2T}, A m^2/kg
20	9.8	2.11	44.33
200	8.3	2.07	52.12
250	8.9	2.38	49.90
300	8.9	2.38	50.45
400	8.4	2.59	53.24
500	8.2	2.99	59.48
600	12.2	5.72	63.29
700	15.1	10.94	70.30
800	13.9	11.10	63.23
900	11.1	5.56	40.54

Magnetic Properties

Specific magnetization in a field of 1600 kA/m (σ_{2T}), specific residual magnetization (σ_r), and coercive force (H_{ci}) of the HMCS powders in the initial state (after 15 h of grinding and 30 min of annealing in the temperature range of 200 to 900°C) are presented in Table 2.

The specific magnetization of the HMCS powders measured in a field of 1600 kA/m (σ_{2T}) changed nonmonotonously with respect to the annealing temperature (Fig. 7) and the effective volume fraction of the magnetite phase (Fig. 8), while the behavior of the specific magnetization attributed to the volume fraction of Fe_3O_4 in the powders (the dotted lines in Figs. 7 and 8) is linear. We may assume the observed differences result from not considering the amorphous phase. We can therefore bring the volume fraction of magnetite into line with the experimental values of σ_{2T} (the group of points on dependence $\sigma_{2T}(T_{ann})$ at $T_{ann} >$ 650°C, fitted by line *2* in Fig. 8) using the analytical expression for line *1* (Fig. 8) on dependence $v_{Fe_3O_4}(T_{ann})$ when $T_{ann} <$ 650°C. The content of the

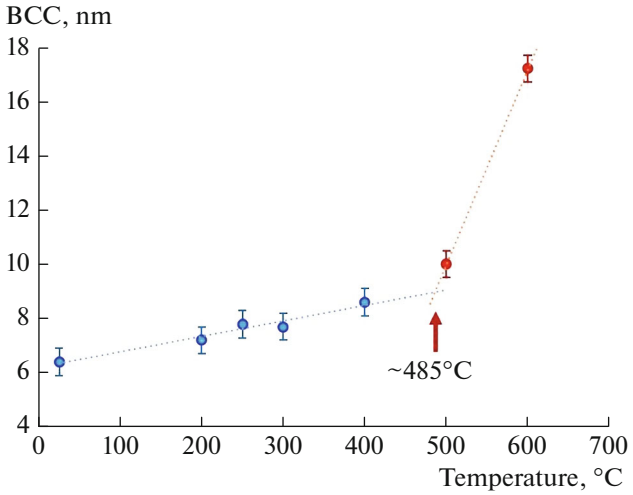

Fig. 4. Changes in the parameters of the BCC of the main phase component as a function of the temperature of annealing for the HMCS powders. Here and below, the trends are presented to aid visualization.

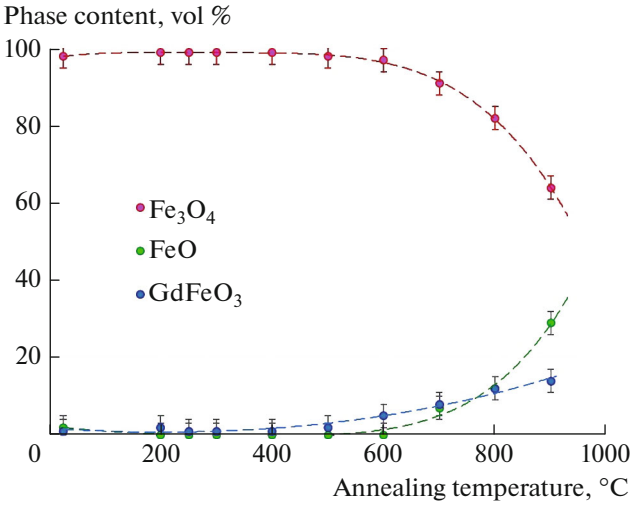

Fig. 5. Changes in the phase composition of the HMCS powders after 30 min of annealing in the temperature range of 200 to 900°C.

amorphous phase in the powders after HMCS is then around 50%[1], and the corrected dependences of the phase composition of the HMCS powders appear as in Fig. 9. Corresponding changes in σ_{2T} as a function of the temperature of annealing are shown in the same figure. In contrast to Fig. 7, dependences $\sigma_{2T}(T_{ann})$ and $v_{Fe_3O_4}(T_{ann})$ in this case correlate with each other very well.

In light of the dependence of the experimental values of the specific magnetization of the HMCS powders on the corrected volume fraction of magnetite $\sigma_{2T}(v_{Fe_3O_4})$ presented in Fig. 10, note they can be fitted with a quadratic function ($R^2 = 0.9978$), provided the obvious condition $\sigma_{2T}(0) \equiv 0$ is met. The resulting value is $\sigma_{2T}(100) = 96.34$ A m^2/kg (calculated curves in Figs. 8–10 are drawn assuming that $\sigma_s(Fe_3O_4) =$ 92 A m^2/kg [21]). The difference between the values of $\sigma_{2T}(100)$ and $\sigma_s(Fe_3O_4)$ is quite large (≈4.7%). Assuming it arises due to the presence of magnetic ions of Gd^{3+} in the magnetite lattice[2], the maximum solubility of gadolinium turns out to be 11.8 at %. This could hardly be achieved, due to an increase in the elastic energy (which is also a quadratic function of concentration). However, the changes shown in Fig. 6 for the magnetite phase lattice parameter accurately represent the line connecting points $a(Fe_3O_4) = 0.8397$ nm and a(11.8 at % Gd) = 0.8428 nm (the dashed line in Fig. 11, calculated by assuming the ionic radii of Gd^{3+} and Fe^{3+} are 0.094 and 0.067 nm, respectively); the maximum experimentally obtained value of $a(x) =$ 0.8433 nm corresponds here to $x \approx 5.14$ at % Gd.

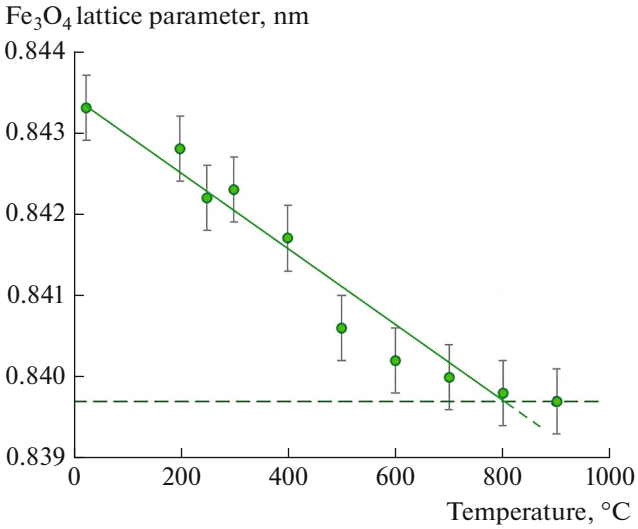

Fig. 6. Dependence of the magnetite phase lattice parameter on the temperature of annealing for the HMCS powders. The dotted line shows the table lattice parameter for Fe_3O_4 ($a = 0.8397$ nm [20]).

[1] Studies of the phase-structural state of the HMCS-powders by high-resolution transmission electron microscopy are being conducted and data will be presented after they are complete.

[2] There are seven electrons in the 4f shell of Gd^{3+}, so $L = 0$, $S = 7/2$, $g = 2$, and $\mu_s = gS = 7\mu_B$. Relatively large Gd^{3+} ions replace Fe^{3+} ions mainly in the octahedral positions of reverse spinel, the magnetic formula of which is [22] $\overline{Fe}^{3+}\left[\overline{Fe}^{3+}\overline{Fe}^{2+}\right]O_4^{2-}$. The cation of Fe^{3+} has five electrons in the 3d shell, so $L = 0$, $S = 5/2$, $g = 2$, and $\mu_s = gS = 5\mu_B$. The difference in the magnetic moment per one substitution is $2\mu_B$. Knowing the difference between the specific magnetizations of alloyed and unalloyed magnetite, we can calculate the limit concentration of the alloying component.

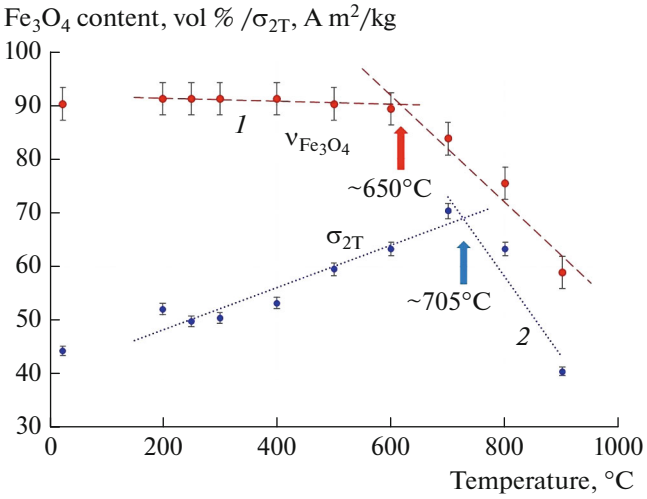

Fig. 7. Dependence of the volume fraction of the magnetite phase (ν_{Fe3O4}) and the specific magnetization of the HMCS-powders in a field of 1600 kA/m (σ_{2T}) on the annealing temperature.

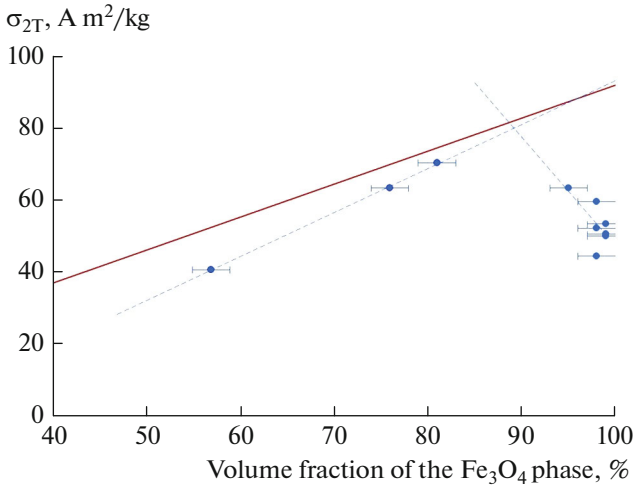

Fig. 8. Changes in the specific magnetization of the HMCS powders, depending on the volume fraction of the magnetite phase. The solid line shows the calculated value of σ_{2T}.

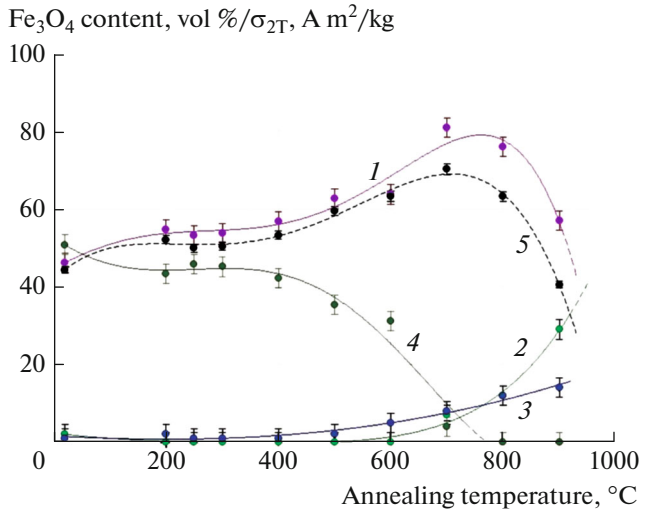

Fig. 9. Adjusted dependences of the volume fractions of the (*1*) magnetite, (*2*) wustite, (*3*) orthoferrite, and (*4*) amorphous phases, and (*5*) behavior of the specific magnetization of the HMCS powders, as a function of the annealing temperature.

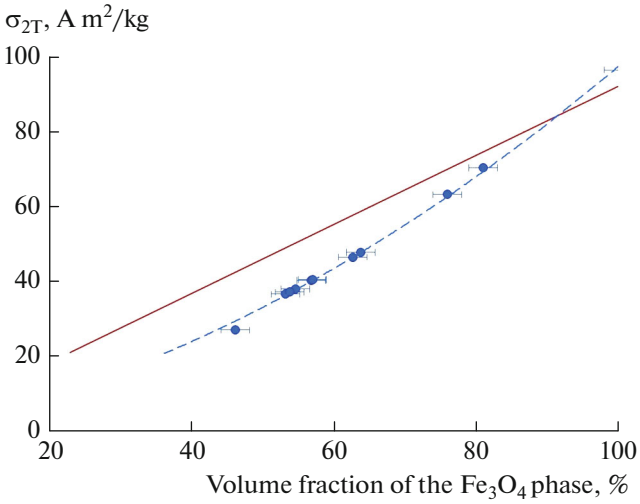

Fig. 10. Dependence of the reduced values of the specific magnetization σ_{2T} of the HMCS powders on the volume fraction of Fe_3O_4.

However, the influence of Gd on the magnetite lattice parameter, demonstrated experimentally in our studies (Fig. 11), disagrees with the conclusions drawn in [16]. Based on X-ray diffraction studies of nanoparticles of magnetite alloyed with Gd (D = 4.74 ± 0.51 nm) obtained by chemical (polyol [2]) means, the authors of [16] stated that "Gd doping did not significantly affect the crystalline of magnetite," since the position of main diffraction peaks of Fe_3O_4 did not change. We suggest (such alloying is possible, according to our studies) that the character of the obtained diffraction spectra (severe line broadening, low signal to background ratio) and probably the low concentration of Gd in the nanoparticles (only a qualitative chemical analysis of alloyed magnetite was done in [16]) did not allow the necessary resolution. In our case, the key result of [16] was that synthesis of this kind is possible, so the quantitative dependences derived here may be regarded as limits in extrapolating the corresponding characteristics of the structure and magnetic properties of Gd-doped magnetite nanoparticles with different sizes in developing chemical means of synthesis.

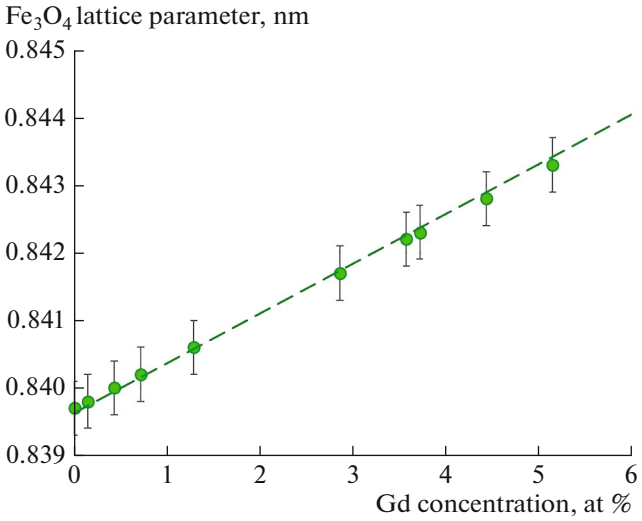

Fig. 11. Calculated dependence of the Fe_3O_4 lattice parameter on the Gd concentration (dashed line) and experimental values measured in this work (according to Fig. 6).

CONCLUSIONS

Comprehensive studies of powders with a nominal composition of 90% [43% Fe_2O_3–57% FeO]–10% Gd_2O_3 in states after 15 h of high-energy ball milling and 30 min of heat treatment in the temperature range of 200–900°C were performed via scanning electron microscopy, X-ray diffraction analysis, differential scanning calorimetry, and measuring hystereses.

It was shown that the main phases in the powders after high-energy ball milling were magnetite (Fe_3O_4) with a lattice parameter 0.4% greater than the corresponding tabular value (a = 0.8397 nm [20]) and the amorphous phase. In addition, the powders were around 2 vol % wustite (FeO) and less than 1 vol % orthoferrite ($GdFeO_3$).

Changes in the phase composition of the HMCS powders during thermal treatment were revealed. No appreciable changes in the phase composition of the HMCS powders were observed in the 200–400°C range of annealing temperatures. Crystallization of the amorphous phase leading to formation of Fe_3O_4 and $GdFeO_3$ phases and a rapid increase in the sizes of the BCC magnetite phase occur from 400 to 700°C. The lattice parameter of Fe_3O_4 falls monotonously and tends to its tabular value in the 200 to 700°C range of annealing temperatures. Annealing at temperatures higher than 700°C leads to a sharp drop in the content of Fe_3O_4 and a simultaneous increase in the volume fractions of FeO and $GdFeO_3$.

Combined analysis of the phase-structural and hysteresis properties of the powders before and after high-energy ball milling and after heat treatment showed that the Gd^{3+} ions dissolved in the Fe_3O_4 lattice by replacing Fe^{3+} in the octahedral sites of the reverse spinel. The maximum experimentally obtained value $a(x)$ = 0.8433 nm corresponds to a Gd content of $x \approx 5.1$ at % (while estimates of the limit solubility of Gd that disregard the elastic energy produce a value of 11.8 at %). The fundamental possibility of obtaining stable magnetite doped with Gd was thus shown. If effective chemical means for its synthesis in a nanosized state are developed, it could become a promising dual T_2–T_1 contrast agent for MRI in the future.

REFERENCES

1. Crozals, G.D., Bonnet, R., Farre, C., and Chaix, C., *Nano Today*, 2016, vol. 11, p. 435.
2. Périgo, E.A., Hemery, G., Sandre, O., et al., *Appl. Phys. Rev.*, 2015, vol. 2, p. 041302.
3. Dadfar, S.M., Roemhild, K., Drude, N.I., et al., *Adv. Drug Delivery Rev.*, 2019, vol. 11, p. 1.
4. Nikitin, A., Fedorova, M., Naumenko, V., et al., *J. Magn. Magn. Mater.*, 2017, vol. 441, p. 6.
5. Gubin, S.P., Yurkov, G.Yu., Koksharov, Yu.A., and Khomutov, G.B., *Russ. Chem. Rev.*, 2005, vol. 74, no. 6, p. 489.
6. Na, H.B. and Hyeon, T., *J. Mater. Chem.*, 2009, vol. 19, p. 6267.
7. Fedorenko, S., Stepanov, A., Zairov, R., et al., *Colloids Surf. A*, 2018, vol. 559, p. 60.
8. Li, Z., Yi, P.W., Sun, Q., *Adv. Funct. Mater.*, 2012, vol. 22, p. 2387.
9. Aime, S., Botta, M., and Terreno, E., *Adv. Inorg. Chem.*, 2005, vol. 57, p. 173.
10. Marckmann, P., Skov, L., Rossen, K., et al., *J. Am. Soc. Nephrol.*, 2006, vol. 17, p. 2359.
11. Kuo, P.H., Kanal, E., Abu-Alfa, A.K., et al., *Radiology*, 2007, vol. 242, p. 647.
12. Bulte, J.W.M. and Kraitchman, D.L., *NMR Biomed.*, 2004, vol. 17, p. 484.
13. Shin, T., Choi, J., Yun, S., et al., *J. Am. Chem. Soc.*, 2014, vol. 8, p. 3393.
14. Keasberry, N.A., Bañobre-López, M., Wood, C., et al., *Nanoscale*, 2015, vol. 7, p. 16119.
15. Domingues, E.M., Tsipis, E.V., Yaremchenko, A.A., et al., *J. Eur. Ceram. Soc.*, 2013, vol. 33, p. 1307.
16. Xiao, N., Gu, W., Wang, H., et al., *J. Colloid Interface Sci.*, 2014, vol. 417, p. 159.
17. Shelekhov, E.V. and Sviridova, T.A., *Met. Sci. Heat Treat.*, 2000, vol. 42, no. 8, p. 309.
18. Shakh-Nazaryan, N., *Izuchenie vliyaniya mekhanicheskoi aktivatsii pri tverdofaznom sinteze keramiki. Uchebno-metodicheskoe posobie* (Studying the Effect of Mechanical Activation in Solid-Phase Synthesis of Ceramics. Study Guide), Rostov-on-Don: Yuzhn. Fed. Univ., 2009, p. 10.
19. Kubaschewski, O., *Iron Binary Phase Diagrams*, Springer, 1982, p. 79.
20. Teja, A.S. and Koh, P.Y., *Prog. Cryst. Growth Charact. Mater.*, 2009, vol. 55, p. 22.
21. Arévalo, P., Isasi, J., Caballero, A.C., et al., *Ceram. Int.*, 2017, vol. 43, p. 10333.
22. Krinchik, G.S., *Fizika magnitnykh yavlenii* (The Physics of Magnetic Phenomena), Moscow: Mosk. Gos. Univ., 1976.

Translated by S. Efimov